

Geophysical Research Letters

RESEARCH LETTER

10.1002/2017GL074532

Key Points:

- NASA's MERRA-2 reanalysis is a publicly available, high-resolution (50 km) data set
- The MERRA-2 reanalysis with assimilated O₃ captures the fine-scale features of stratospheric intrusions known to impact surface air quality
- The combination of meteorological variables and ozone may provide a valuable and unique tool for air quality managers

Correspondence to:

K. E. Knowland,
k.e.knowland@nasa.gov

Citation:

Knowland, K. E., Ott, L. E., Duncan, B. N., & Wargan, K. (2017). Stratospheric intrusion-influenced ozone air quality exceedances investigated in the NASA MERRA-2 reanalysis. *Geophysical Research Letters*, 44, 10,691–10,701. <https://doi.org/10.1002/2017GL074532>

Received 13 JUN 2017

Accepted 2 SEP 2017

Accepted article online 7 SEP 2017

Published online 21 OCT 2017

Stratospheric Intrusion-Influenced Ozone Air Quality Exceedances Investigated in the NASA MERRA-2 Reanalysis

K. E. Knowland^{1,2} , L. E. Ott², B. N. Duncan³, and K. Wargan^{2,4}

¹Universities Space Research Association/Goddard Earth Science Technology & Research, Columbia, MD, USA, ²Global Modeling and Assimilation Office, NASA Goddard Space Flight Center (GSFC), Greenbelt, MD, USA, ³Laboratory for Atmospheric Chemistry and Physics, NASA GSFC, Greenbelt, MD, USA, ⁴Science Systems and Applications, Inc., Lanham, MD, USA

Abstract Stratospheric intrusions have been the interest of decades of research for their ability to bring stratospheric ozone (O₃) into the troposphere with the potential to enhance surface O₃ concentrations. However, these intrusions have been misrepresented in models and reanalyses until recently, as the features of a stratospheric intrusion are best identified in horizontal resolutions of 50 km or smaller. NASA's Modern-Era Retrospective Analysis for Research and Applications Version-2 (MERRA-2) reanalysis is a publicly available high-resolution data set (~50 km) with assimilated O₃ that characterizes O₃ on the same spatiotemporal resolution as the meteorology. We demonstrate the science capabilities of the MERRA-2 reanalysis when applied to the evaluation of stratospheric intrusions that impact surface air quality. This is demonstrated through a case study analysis of stratospheric intrusion-influenced O₃ exceedances in spring 2012 in Colorado, using a combination of observations, the MERRA-2 reanalysis and Goddard Earth Observing System Model, Version 5 simulations.

1. Introduction

Surface ozone (O₃) is harmful to human health and agriculture (Kryzanowski & Cohen, 2008; Scherrer et al., 2006). Near the surface, O₃ is termed a secondary pollutant since it is a product of the photochemical reaction with precursors such as nitrogen oxides (NO_x; NO and NO₂), carbon monoxide (CO), and nonmethane hydrocarbons which have both man-made and natural emission sources in the troposphere. Therefore, in order to reduce near-surface O₃ concentrations, communities must reduce anthropogenic pollution sources. However, the injection of stratospheric O₃ into the troposphere, known as a stratospheric intrusion (SI), can also lead to concentrations of ground-level O₃ exceeding the national ambient air quality standard (NAAQS) set by the Environmental Protection Agency (EPA), especially at high elevations (e.g., Langford et al., 2009, 2015; Lin et al., 2012, 2014; Yates et al., 2013; Zhang et al., 2014). In October 2015, the EPA revised the U.S. NAAQS for daily maximum 8 h average (MDA8) O₃ from 75 parts per billion by volume (ppbv) to 70 ppbv (U.S. Environmental Protection Agency, 2015). Therefore, it is crucial that we are able to understand, model, and predict SIs and their potential impact on surface O₃ concentrations.

SIs form as a result of the tropopause being drawn down below the jet stream, referred to as tropopause folding, often associated with an upper level trough. SIs are characterized by O₃-rich (e.g., Browning, 1997; Danielsen, 1968; Holton et al., 1995; Shapiro, 1974, 1980) and CO-poor (Fischer et al., 2000) air, with relatively high levels of potential vorticity (PV) (Holton et al., 1995) and low levels of water vapor often observed in satellite imagery as a "dry slot" (e.g., Bader et al., 1995; Wimmers et al., 2003). Therefore, tropopause folds can lead to the mixing of stratospheric and tropospheric air with different chemical and meteorological properties at low altitudes (e.g., Danielsen, 1980; Holton et al., 1995; Shapiro, 1980);, remaining behind a midlatitude cyclone's surface cold front (Bethan et al., 1998; Browning, 1997; Cooper et al., 2001; Knowland et al., 2015). The West Coast of the USA is located at the end of the Pacific Ocean storm track (e.g., Hoskins & Hodges, 2002), a region favorable for stratosphere-to-troposphere transport of O₃ (James et al., 2003; Škerlak et al., 2014; Sprenger & Wernli, 2003; Stohl et al., 2003). On the leeside of the Rocky Mountains, cyclones form (or redevelop) supported by upper level troughs (Carlson, 1991; McClain, 1960). However, the descending motion associated with the upper level trough can still be a strong feature in the troposphere over the Rocky Mountains,

prior to the identification of a surface low-pressure system. In the upper level flow, the troughs can form closed lows and even become “cutoff” from the westerly flow (Palmén & Newton, 1969). This can result in the prolonged influence of the tropopause folds on tropospheric O₃ concentrations over a region (Lin et al., 2012; Yates et al., 2013) until the cutoff low (COL) dissipates or is reabsorbed into the mean flow (Nieto et al., 2008). During the winter and spring, there is a buildup of O₃ in the lower stratosphere, and this leads to SIs having the largest influence on surface O₃ in the spring (Danielsen & Mohnen, 1977; Holton et al., 1995; Monks, 2000).

For over 40 years, studies have observed the injection of O₃-rich air into the troposphere within tropopause folds over western USA (e.g., Cooper et al., 2004; Langford et al., 1996, 2009, 2012; Lefohn et al., 2011; Lovill, 1970; Shapiro, 1980; Wimmers et al., 2003) with recent studies focusing on the impact of SIs on O₃ air quality exceedances in the high-elevation communities of the Rocky Mountains (e.g., Langford et al., 2009, 2015; Lin et al., 2012, 2014; Yates et al., 2013; Zhang et al., 2014). Langford et al. (2009) focused on the transport of stratospheric O₃ in Colorado’s Front Range during the spring of 1999 using lidar and surface measurements of O₃. They identified high concentrations of O₃ in the midtroposphere down to the surface as a result of tropopause folds associated with upper level troughs in the region. Lin et al. (2012) utilized the abundance of vertical observations from ozonesondes and lidar taken during the 2010 NOAA CalNex field campaign in California as well as ground-based measurements throughout western USA, in conjunction with a model study to quantify the stratospheric fraction of air that impacts NAAQS exceedance events. Using the NOAA Geophysical Research Laboratory Atmosphere Model version 3 (AM3) with fully coupled stratosphere-troposphere chemistry at ~50 km resolution, Lin et al. (2012) attributed 50–60% of total modeled surface O₃ in spring 2010 (as much as 20–40 ppbv of additional O₃ during four deep intrusions) to stratospheric origins on exceedance days. Using a coarser resolution model (~200 km), Lin et al. (2015) extended the analysis to April and May during a 23 year period (1990–2012) and found that the average stratospheric O₃ contribution is 15–25 ppbv of western U.S. surface O₃.

While the impact of SIs on surface O₃ in the western U.S. is well documented, simulating and predicting such events remains challenging. The resolutions of current global meteorological analyses (~10–50 km) are sufficient for resolving the dynamical evolution of SIs; however, these models typically contain very limited representations of trace gases like O₃. Reanalyses have been used in numerous studies to explore the frequency, spatial variations, and structure of SIs (e.g., Lefohn et al., 2011; Nath et al., 2016; Sprenger & Wernli, 2003; Stohl & Trickl, 1999; Reutter et al., 2015; Waugh & Polvani, 2000); however, there are very few such studies which also use reanalysis O₃ (Knowland et al., 2015, 2017; Ott et al., 2016; Ryoo et al., 2017; Škerlak et al., 2014; Zanis et al., 2014). It is our objective to investigate whether NASA’s Modern-Era Retrospective Analysis for Research and Applications Version-2 (MERRA-2) reanalysis, which is similar to NASA’s Global Modeling and Assimilation Office (GMAO) operational forecasting system, is able to capture the dynamical features of a SI, in particular, the isentropic descent of elevated O₃ within and below the tropopause fold. Such data sets would support air quality agencies for more rapid identification of the impact of stratospheric air on ground-level O₃ (Kaldunski et al., 2017) separate from local sources or the long-range transport of O₃ (Ryoo et al., 2017). The focus of this study will be on springtime (March–June (MAMJ)) O₃ air quality exceedances in 2012 which were identified by the EPA as having direct connection with SIs (US EPA AQS database, 2017).

2. Data

2.1. Observational Data Sets

In the spring of 2012, there were 7 days when the MDA8 O₃ (EPA AirData, 2016) at the Rocky Mountain National Park (RMNP) Long’s Peak monitoring station (40.27° N, 105.54° W, 2,742 m, Air Quality System (AQS) Site ID 08-069-0007, located ~100 km northwest of Denver) exceeded the NAAQS of 75 ppbv as a result of SIs (US EPA AQS database, 2017): 26 March, 6 April, 27 April, 26–28 May, and 14 June. Several other suburban and rural monitoring stations in Colorado also reported exceedances related to SIs on these and other dates in spring 2012 (US EPA AQS database, 2017). Less than half of the diurnal variation in the hourly MAMJ O₃ at RMNP can be explained by the first (diurnal) harmonic; therefore, other drivers in the O₃ variability must be considered. Deep SIs, those which impact surface O₃ concentrations, were anomalously frequent in the western USA in the spring of 2012 compared to the 1990–2012 period (Lin et al., 2015), and observed MDA8 O₃ was also found to have a maximum in the western USA that spring for the period 2004–2012 (Baylor et al., 2016). This study will explore the representation of two of the SIs in remote sensing observations and the Goddard Earth Observing System Model, Version 5 (GEOS-5) model and assimilation products. The first case study in early

spring (26 March local time (LT; +07:00 UTC) hereafter will be referred to as the SI-1 event and the second case study, which occurred in late spring (26–28 May event LT), will be referred to as the SI-2 event.

Daily total column O₃ (TCO) and relative humidity (RH) from the Atmospheric Infrared Sounder (AIRS) on NASA's Aqua satellite are used to identify the presence of SIs over RMNP in observational data and to validate MERRA-2 reanalysis TCO since the AIRS O₃ data were not assimilated in MERRA-2. AIRS is equipped to measure both meteorological variables and chemical profiles (Aumann et al., 2003; Chahine et al., 2006; Susskind et al., 2006) and observes the surface twice daily (01:30 and 13:30 LT). The retrievals are performed even when clouds are present which makes the data set ideal when analyzing regions near midlatitude cyclones. The AIRS team produces several data sets of different spatiotemporal resolution. We use the level 3 version 6 (L3 V6) at 1° horizontal resolution (AIRS Science Team/Joao Texeira, 2013).

2.2. Model Data Sets

NASA's MERRA-2 reanalysis is an ideal candidate to explore the vertical structure of the SIs over RMNP as it is a publicly available, high-resolution reanalysis data set ($0.5^\circ \times 0.625^\circ$ latitude-by-longitude grid, nominally ~ 50 km in the latitudinal direction, 72 model layers up to 0.01 hPa (Bosilovich et al., 2016; Gelaro et al., 2017)) which assimilates both O₃ and meteorological observations (Bosilovich et al., 2015; Gelaro et al., 2017; McCarty et al., 2016). The MERRA-2 reanalysis covers the period from 1 January 1980 to within a couple weeks of real time and is the product of the GEOS-5 data assimilation system (Bosilovich et al., 2015; Gelaro et al., 2017). The GEOS-5 model includes monthly averaged ozone production and loss rates linearly interpolated to daily values for both the stratosphere and the troposphere (Bosilovich et al., 2016). After 2004, MERRA-2 assimilates satellite retrievals of TCO from the Ozone Monitoring Instrument (Levelt et al. (2006)) and stratospheric O₃ profiles from the Microwave Limb Sounder (Waters et al. (2006)) (Bosilovich et al., 2015; Gelaro et al., 2017; McCarty et al., 2016). MERRA-2 O₃ in the lower stratosphere is well represented and has been shown to agree with ozonesondes (Wargan et al., 2015, 2017); therefore, where there is direct influence of stratospheric O₃ into the troposphere, such as an SI, we can expect realistic intrusions although possibly biased since the background ozone in the troposphere is simulated by simple chemistry parametrization (Ott et al., 2016).

The meteorological and chemical variables—winds (u, v), vertical velocity (ω), equivalent potential temperature (θ_e ; calculated from temperature and specific humidity), Ertel's PV, RH and O₃ mixing ratios—were extracted on pressure levels up to 150 hPa (Global Modeling and Assimilation Office (GMAO), 2015a). In addition, MERRA-2 sea level pressure (SLP) (GMAO, 2015b) and TCO (GMAO, 2015c) are used in the comparison to the AIRS retrievals.

Two additional model variables are used: GEOS-5 simulated CO using emissions described in Ott et al. (2010) and an idealized stratospheric “influence” tracer (STFR) from Ott et al. (2016). The STFR is set to 1 in the stratosphere and to 0 at the surface. For the STFR simulation, the tropopause was the higher height of the thermal tropopause or the dynamical tropopause. In the GEOS model, the dynamical tropopause is defined as the 3 potential vorticity unit (PVU) isosurface, where 1 PV unit (PVU) = $10^{-6} \text{ K m}^2 \text{ kg}^{-1} \text{ s}^{-1}$, which is higher than the conventional 2 PVU isosurface (Holton et al., 1995).

3. Results

The 8 h running average O₃ and the hourly average O₃ observed at RMNP and the corresponding 3-hourly surface O₃ from MERRA-2 (GMAO, 2015d) are presented here for spring of 2012 (Figure 1b). During the SI-1 event, the observed hourly O₃ at RMNP ≥ 75 ppbv for 7 h (1 h on 26 March and 6 h on 27 March, based on UTC, Figure 1a) with the maximum observed hourly O₃ equal to 87 ppbv observed at 27 March 2012 00UTC (Figure 1b; MERRA-2 O₃ = 58 ppbv). The second intrusion event, SI-2, influenced ground-level O₃ for several days at RMNP; observed hourly O₃ ≥ 75 ppbv for 11 h during this 3 day period (Figure 1a) with maximum observed hourly O₃ of 91 ppbv at 09 UTC on 27 May 2012 (Figure 1b; MERRA-2 O₃ = 65 ppbv). Considering the new NAAQS value for MDA8 O₃, RMNP observed hourly O₃ ≥ 70 ppbv for 11 h during the SI-1 event and 30 h for the SI-2 event (Figure 1a). Figure 1 highlights the doubling of possible exceedance days if the new MDA8-O₃ NAAQS of ≥ 70 ppbv is applied to 2012. As expected, the MERRA-2 surface O₃ for the grid box closest to RMNP underestimates the O₃ variability of a point source measurement ($r^2 = 0.34$, based on 968 3-hourly time steps; Figure 1b) in part because of the simple O₃ chemistry in the GEOS-5 model; however, there are spikes in the reanalysis O₃ at or near the times of observed O₃ exceedances, portraying the influence of stratospheric O₃ on the grid box.

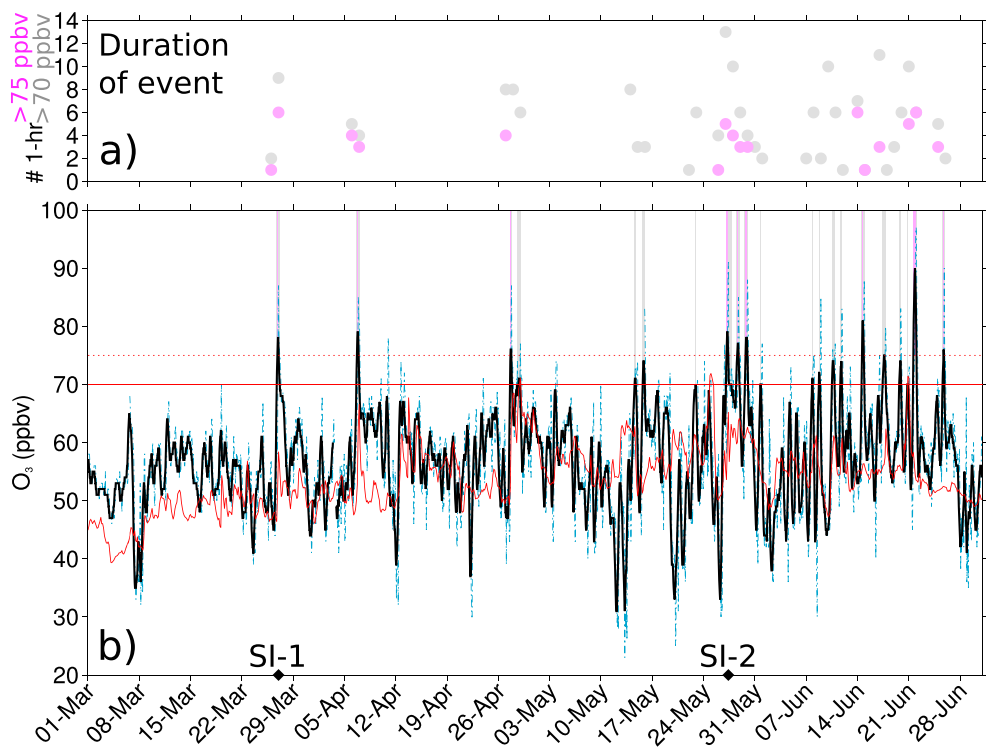
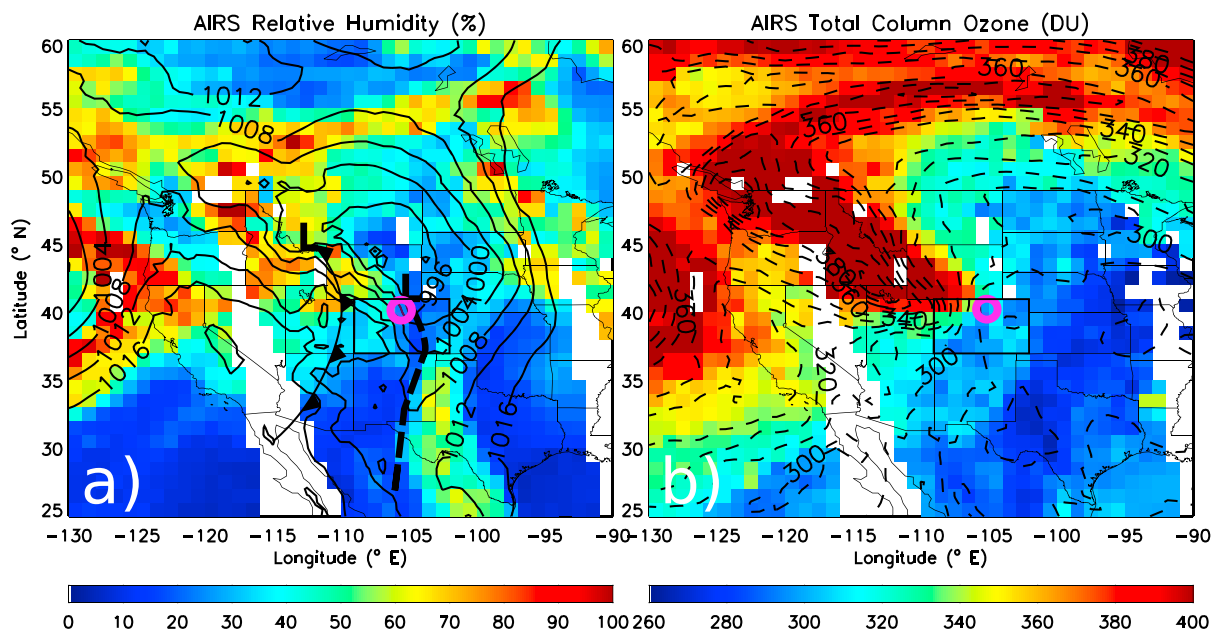


Figure 1. (a) Number of hours in an exceedance day (time in UTC) where the RMNP observed hourly average $O_3 \geq 75$ ppbv (pink circles) and ≥ 70 ppbv (grey circles); (b) 8-hourly running average O_3 (solid black line) and hourly average O_3 (dash-dotted blue line) from the EPA surface observations at RMNP and the 3-hourly MERRA-2 reanalysis surface O_3 at the nearest grid point to RMNP (40°N , 105.625°W ; red contour line) for 1 March to 30 June 2012 (time in UTC). The exceedance events where the MDA8 $O_3 \geq$ the EPA standard in 2012 (75 ppbv; dotted horizontal red line) are indicated by the vertical pink shading, and the events that would be considered exceedances under the new EPA standard (70 ppbv; solid horizontal red line) are indicated by the vertical grey shading. The times of the SI-1 and SI-2 events, corresponding to Figures 2–4, are indicated by the black diamonds.

At the time of an intrusion, relatively dry air is expected to descend toward the surface behind a cold front (e.g., Bethan et al., 1998; Cooper et al., 2001; Knowland et al., 2015). Due to the topography, SLP over the Rocky Mountains can be difficult to interpret; however, both of the SI case studies occurred when there was a low pressure in the Northern Plains region (Figures 2a and 2c). During the SI-1 event, there were two low-pressure systems, one in southwest Montana and one in southeast Wyoming (Figure 2a). The 700 hPa RH was low to the west of a surface trough extending from Wyoming approximately due south into Mexico. For the late spring SI-2 event, a cyclone tracked northeastward into North Dakota with a cold front trailing into western Kansas where it transitions to a stationary front (Figure 2c). Here a new low-pressure system formed in southeastern Colorado, from which a dry line extends southward through Texas. While relatively low RH is observed by AIRS to the west of the cold front through the Dakotas and Nebraska, there is an even stronger gradient in RH across the dry line (Figure 2c).

The SI events can be identified by concurrent observations of O_3 -rich air with the low RH. This can be achieved by focusing on regions where the gradients in TCO are large (Olsen et al., 2000; Ott et al., 2016). The spatial distributions in AIRS TCO and MERRA-2 TCO at the approximate time of the AIRS observations agree well (Ott et al., 2016), although the MERRA-2 TCO is generally biased low compared to observations in Figures 2b and 2d. This aligns with the findings of Wargan et al. (2017) that MERRA-2 TCO in the midlatitudes was biased low compared to independent TCO measurements from the TOMS (Total Ozone Mapping Spectrometer; Herman et al., 1991) instrument. The maximum TCO—in both AIRS and MERRA-2—stretches from the Pacific Northwest into the Rocky Mountain states linearly in Figure 2b and with curvature in Figure 2d. The location of large TCO gradients in Figures 2b and 2d corresponds to the low-RH regions in Figures 2a and 2c; in particular, large TCO gradients in both AIRS and MERRA-2 and low RH are colocated over Colorado (Figure 2).

SI-1



SI-2

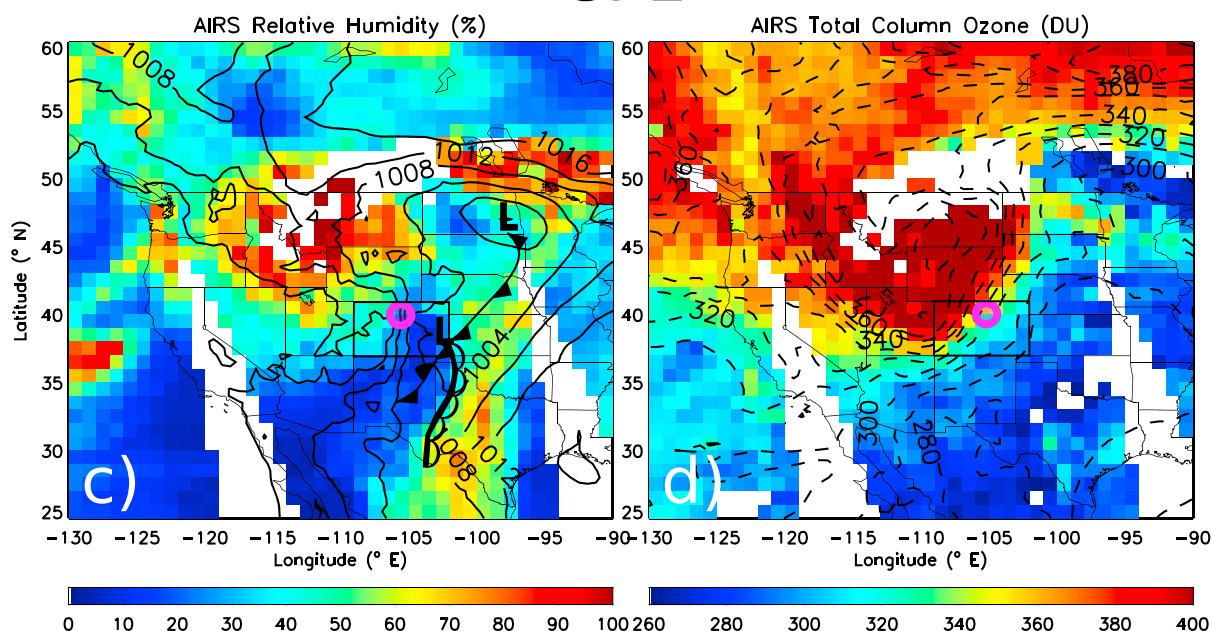


Figure 2. (a and c) AIRS 700 hPa RH (color; %) with MERRA-2 SLP (4 hPa intervals) and (b and d) TCO from AIRS (color; Dobson unit (DU)) and MERRA-2 (dashed; 10 DU intervals) for (Figures 2a and 2b) SI-1 and (Figures 2c and 2d) SI-2. The approximate location of low-pressure centers (L) and frontal boundaries—cold front (line with filled triangles (Figures 2a and 2c), surface trough (dashed line (Figure 2a), stationary front (filled triangles and half circles on opposite sides of line (Figure 2c)), dry line (line with open half circles (Figure 2c)—are presented from the 18 UTC surface analysis (close to 13:30 LT pass) on (Figure 2a) 26 March 2012 and (Figure 2c) 27 May 2012 (www.wpc.ncep.noaa.gov/archives/web_pages/sfc/sfc_archive_maps, Accessed 8 November 2016). Note, not all fronts from the analysis archives have been depicted. The location of RMNP (pink open circle) and the Colorado state border (thin black line) are emphasized.

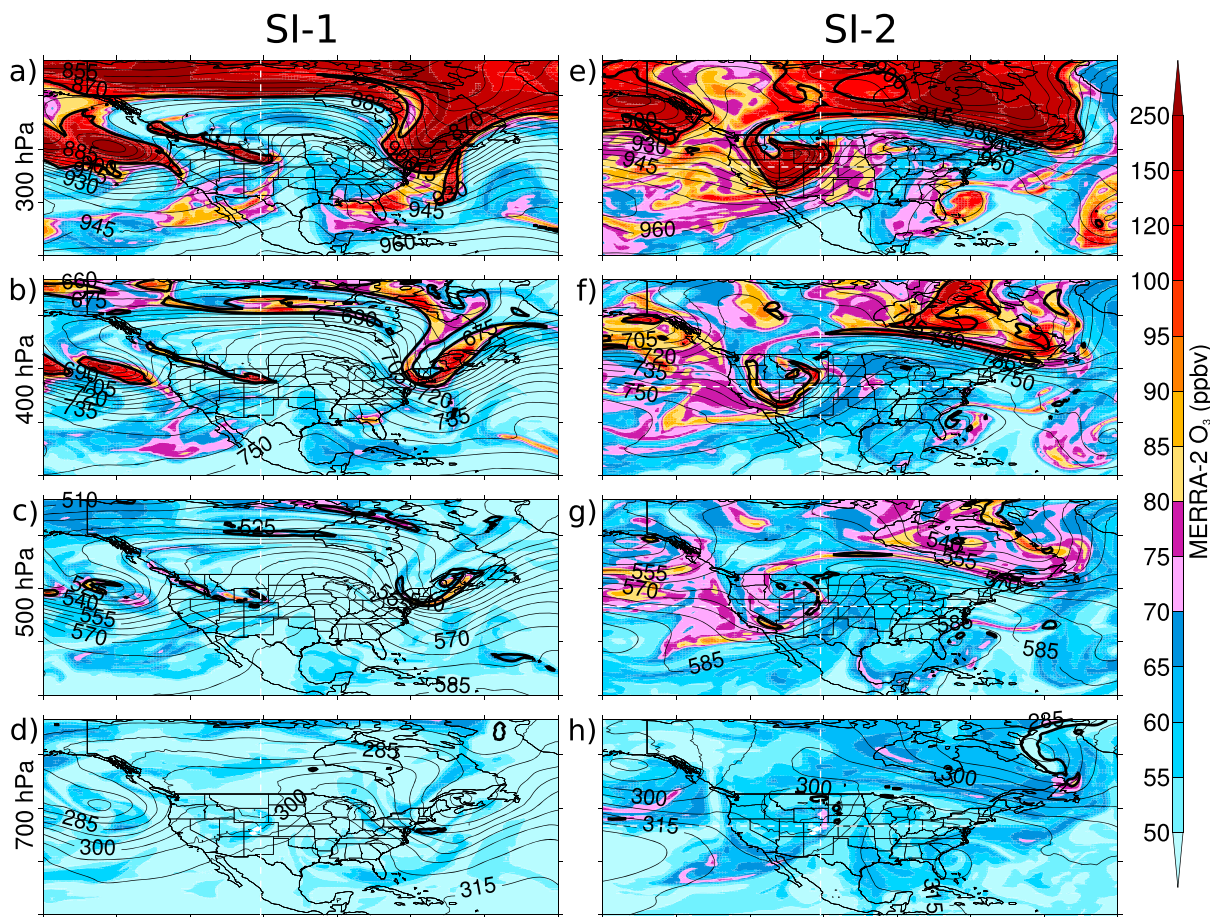
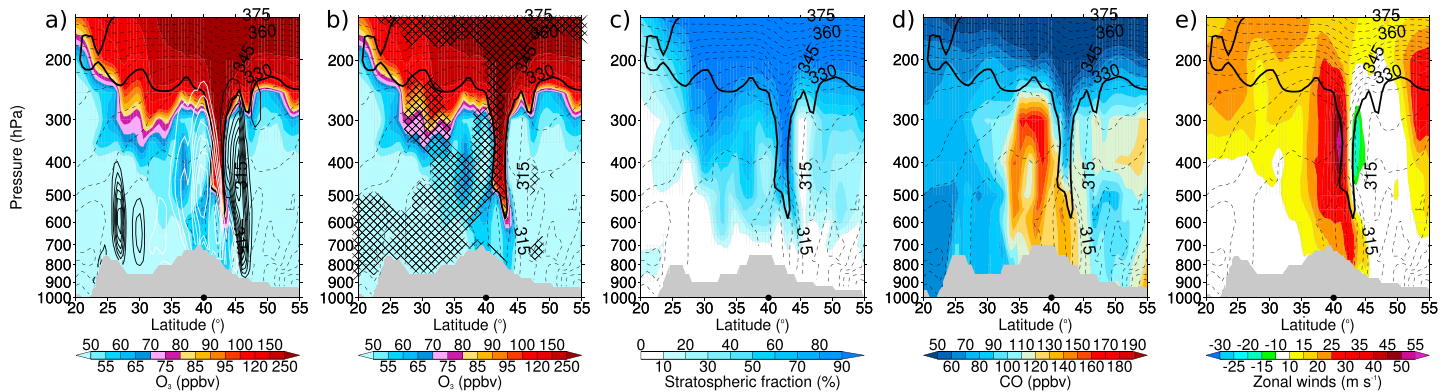


Figure 3. O₃ distribution (color; 5 ppbv increments up to 100 ppbv and increment size increases above 100 ppbv), geopotential height (thin black contours; 5 decameter intervals) and dynamical tropopause (2 PVU isosurface; thick black contour) on (a and e) 300, (b and f) 400, (c and g) 500, and (d and h) 700 hPa surfaces corresponding to the time of maximum O₃ observations at RMNP during the SI-1 event (27 March 2012 00 UTC; Figures 3a–3d) and the SI-2 event (27 May 2012 09 UTC; Figures 3e–3h). Light and dark pink color intervals highlight the previous and current EPA O₃ standard, respectively. The white dashed lines correspond to transects in Figure 4.

We look for further evidence of the SI-1 and SI-2 tropopause folding events in the MERRA-2 reanalysis at the time of maximum O₃ at RMNP (Figure 3). From 300 to 500 hPa over the western USA, there are fine-scale filaments of stratospheric air, specifically high levels of O₃ within the 2 PVU contour, which distinguish the SI events from the background (Figure 3). At the time of maximum hourly O₃ observed at RMNP during the SI-1 and SI-2 events, the SI-1 is linear—stretching from Vancouver Island, Canada, to the Wyoming–Colorado border—as opposed to the curved SI-2 from Washington down to Arizona and back to Montana (400 hPa, Figure 3). Both SI events are a result of a cutoff low (COL) near the West Coast of the USA in the days prior to the O₃ exceedances (not shown). Prior to the exceedance at RMNP as a result of SI-1, the tropopause fold rotates around the COL and at 500 hPa has a hooked shape off the coast of California (not shown) before becoming deformed and elongated—impacting RMNP—as the center of vorticity moves east and the western portion is being pulled west as a consequence of an Aleutian low (Figures 3a–3d). The hook shape of the SI-2 led to the longer period of high O₃ (≥ 75 ppbv) at RMNP compared to the duration of high O₃ observations associated with SI-1; as the SI-2 fold continued to rotate over the western USA at the end of May, there was continued draw down of stratospheric air toward the surface over the area, unlike the SI-1 event which was steered to the northeast as it decayed. It is worth noting that the tropospheric background levels of MERRA-2 O₃ are qualitatively consistent with a seasonal increase in photochemical production from March (Figures 3a–3d) to May (Figures 3e–3h).

The intrusion of air from the stratosphere into the troposphere is captured in vertical transects for the SI events in the MERRA-2 reanalysis data set and supported by the additional GEOS-5 CO and a fraction of stratospheric

SI-1



SI-2

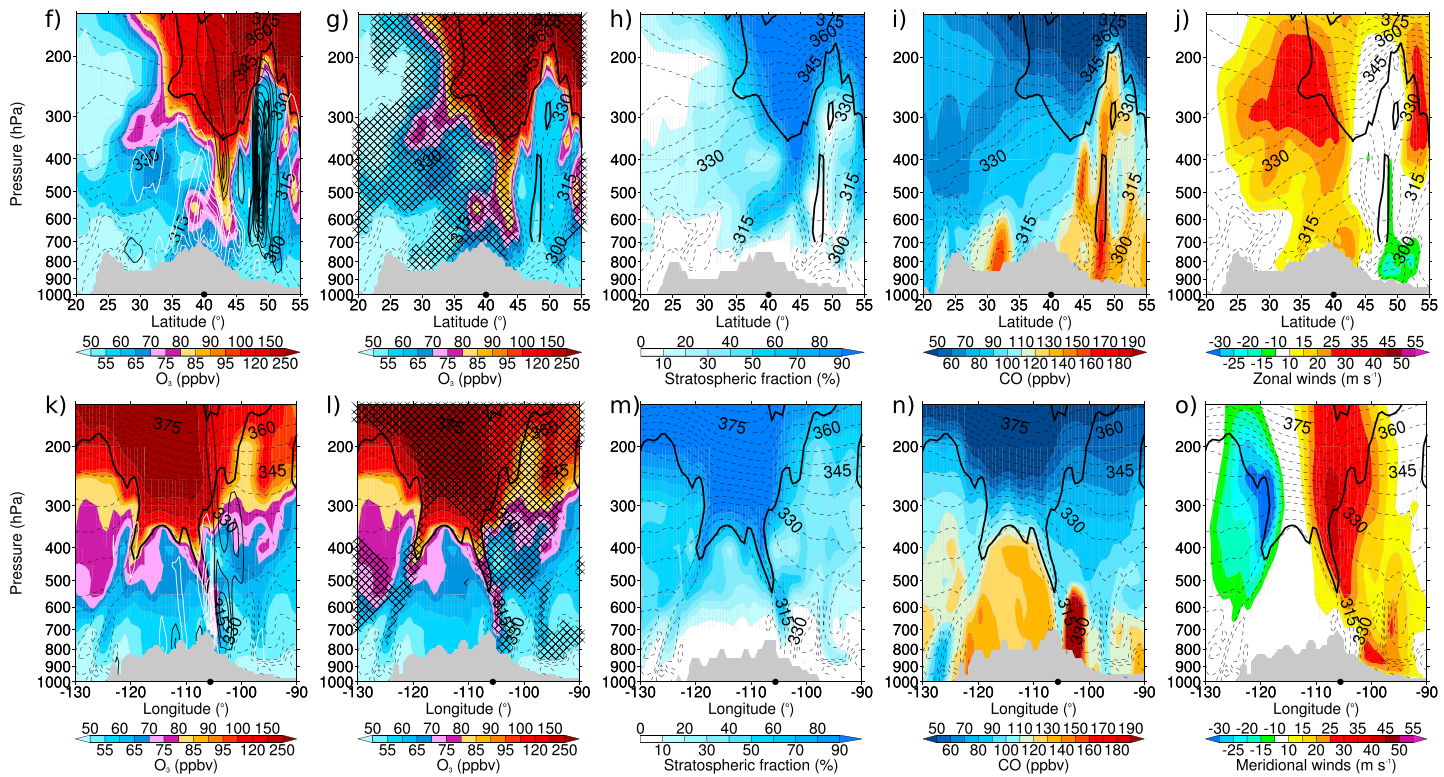


Figure 4. Vertical transects of (a–e) the SI-1 event and (f–o) the SI-2 event taken at the times of maximum O₃ observation at (Figures 4a–4j) 105.625° W from 20° to 55° N over RMNP (black dot, 40° N) and (Figures 4k–4o) 40° N from 130° to 90° W over RMNP (black dot, 105.625° W). O₃ (Figures 4a, 4b, 4f, 4g, 4k, and 4l; ppbv), stratospheric fraction (Figures 4c, 4h, and 4m; %), CO (Figures 4d, 4i, and 4n; ppbv), zonal winds (Figures 4e and 4j; m s⁻¹), and meridional winds (Figure 4o; m s⁻¹) are all shown in color with θ_e (dashed contour lines, 5 K intervals) and the isosurface of 2 PVU (thick black contour). In addition, ω (Figures 4a, 4f, and 4k; solid contour lines, 10 hPa h⁻¹ intervals, with white contours for descent and black contours for ascent) and RH (Figures 4b, 4g, and 4l; hatching <30%) are drawn. Orography indicated by grey region.

air tracer (STFR) data (Figure 4). In the North-South (N-S) transect through SI-1, the dynamical tropopause and high O₃ (>85 ppbv, Figures 4a and 4b; >40% STFR, Figure 4c) reached altitudes as low as ~600 hPa, and elevated O₃ (> 55 ppbv) reached the surface. Relatively dry air is found within the tropopause fold and in the troposphere to the south of the fold (RH <30 %, Figure 4b). The low CO (<110 ppbv, Figure 4d) reached 500 hPa within the tropopause fold; however, since the gradient in CO at the base of the fold is less than

the gradient of O_3 , the influence of stratospheric CO was lost due to mixing with tropospheric air characterized by higher CO mixing ratios. A strong jet at 350 hPa ($u > 50 \text{ m s}^{-1}$, Figure 4e) connects down to the surface. There is also a clear frontal boundary on the northside of the fold extending from an upper level front (indicated by tight isotherms, Figures 4a–4e) down to the surface with strong descent ($\omega > 80 \text{ hPa h}^{-1}$, white contours, Figure 4a) and strong ascent ($\omega < -80 \text{ hPa h}^{-1}$, black contours, Figure 4a).

Both N-S and West-East (W-E) transects are shown for the SI-2 case study (Figures 4f–4o). Although the N-S transect is shown to be just on the eastern edge of the tropopause fold (Figures 3e–3h) and the tropopause does not appear to be depressed below 350 hPa over RMNP (Figures 4f–4j), there are still strong indicators of a fold in the region. Specifically, between 35° and 45° N, there are increased levels of O_3 reaching the surface (>65 ppbv, Figures 4f and 4g) within an area marked by strong descent ($\omega > 60 \text{ hPa h}^{-1}$, Figure 4f), low humidity ($RH < 30\%$ south of 45° N, Figure 4g), large STFR (>60% at 600 hPa, Figure 4h), and low CO (<110 ppbv, Figure 4i). The frontal boundary can be identified by the large gradients of ω and θ_e to the north of RMNP. This transect highlights the ascent ahead of the front (reaching up to ~200 hPa at 50° N, maximum $\omega < -120 \text{ hPa h}^{-1}$ at 400 hPa) and to a lesser extent the descent behind the front (Figure 4f).

Due to the curvature of the SI-2 fold, the W-E transect intersects both sides of the hook as seen at 400 hPa in Figure 3f. The W-E transect captures the tropopause fold at 105° W over RMNP reaching 550 hPa as well as the western portion of the fold reaching below 400 hPa at 120° W (Figures 4k–4o). Figure 4o shows the strong jet on both sides of the curved tropopause fold ($v > 40 \text{ m s}^{-1}$ at 105° W and $v < -30 \text{ m s}^{-1}$ at 120° W). The front above RMNP is also seen in this transect by the large gradients in both ω (Figure 4k) and θ_e (Figures 4k–4o). Specifically, isentropic descent above RMNP brings dry, O_3 -rich air from the stratosphere toward the surface ($O_3 > 80 \text{ ppbv}$ and STFR > 70% at 600 hPa, $O_3 > 65 \text{ ppbv}$ at surface, Figures 4k–4m). It is interesting to note that low CO (<110 ppbv, Figure 4n) is simulated to reach the surface at RMNP, despite the large CO values to the east emitted by a nearby fire. Biomass burning emissions used in the GEOS-5 simulation of CO follow the Quick Fire Emission Data Set version 2.4r6 which is based on Moderate Resolution Imaging Spectroradiometer satellite fire radiative power (Darmenov & da Silva, 2015).

4. Conclusions

Stratospheric intrusions have been the interest of decades of research, especially for the potential influence on ground-level O_3 concentrations. However, until recently, the fine-scale nature of the O_3 filaments have been misrepresented in models and reanalyses, as the features of an SI are best identified in horizontal resolutions of 50 km or smaller (Büker et al., 2005; Lin et al., 2012; Ott et al., 2016). For this reason, and likely because reanalysis O_3 corresponds better with independent observations in the stratosphere than in the troposphere (Dragani, 2011; Wargan et al., 2015, 2017), there are very few studies of stratosphere-to-troposphere transport which use reanalysis O_3 (Knowland et al., 2015, 2017; Ott et al., 2016; Ryoo et al., 2017; Škerlak et al., 2014; Zanis et al., 2014). NASA's MERRA-2 reanalysis is such a high-resolution data set, which benefits from assimilated O_3 to present O_3 on the same spatiotemporal resolution as the meteorology. Here two case study examples of SI events which were known to impact surface O_3 air quality are examined. The SI events are diagnosed by the folding of the tropopause under the jet stream and subsequent isentropic descent of dry, O_3 -rich/CO-poor stratospheric air toward the surface using the MERRA-2 reanalysis in combination with surface O_3 and satellite observations and GEOS-5 simulated CO and a stratospheric tracer. We show that MERRA-2, a publicly available data set, can be used in scientific studies to identify SIs by both atmospheric dynamics and composition. This is a proof of concept study opening the door to detailed multiyear analyses of stratospheric intrusions over the USA and worldwide. Though the MERRA-2 reanalysis tends to underestimate the magnitude of surface O_3 during the SIs (see also Ott et al., 2016), the combination of meteorological variables and O_3 for a relatively long period of time to within a few weeks of present time may provide a valuable and unique tool for air quality managers (Kaldunski et al., 2017) and scientific studies of stratospheric intrusions.

It is important to be able to identify the differences in anthropogenic and natural sources of O_3 , especially on exceedance days. Since the GEOS-5 model used to produce MERRA-2 does not simulate full O_3 chemistry in the troposphere, we are unable to determine the influence of stratospheric O_3 on surface concentrations separate from photochemically produced O_3 , especially in late spring/early summer. The impact of photochemically produced O_3 on total O_3 later in the spring will be explored in more detail using the GEOS-5 chemistry climate model in a future publication. Yet this study presents strong evidence that the MERRA-2 reanalysis can be used in the identification of SIs.

Acknowledgments

K. Emma Knowland's analysis of MERRA-2 was supported through GMAO core funding administered by NASA's Modeling, Analysis, and Prediction Program. Implementation of STFR in GEOS-5 was funded by NASA's Atmospheric Composition Campaign Data Analysis and Modeling program. The MERRA-2 reanalysis data and the AIRS satellite data (AIRX3STD_V006) are available through the NASA GES DISC online archive (<https://disc.gsfc.nasa.gov/>). Tables of the hourly and 8-hourly average O₃ observations are available to download on the EPA's website (http://aqsdri.epa.gov/aqsweb/aqstmp/airdata/download_files.html). The authors would like to acknowledge Brad Weir for providing the GEOS-5 simulation of CO. The GEOS-5 CO and STFR data will be provided upon request by Lesley Ott. The authors would like to thank Pat Reddy for providing the initial list of SI candidates in 2012 and Richard Payton for amassing the list of stratospheric intrusions from the EPA AQS database.

References

- AIRS Science Team/Joao Texeira (2013). *AIRS/Aqua L3 Daily Standard Physical Retrieval (AIRS+AMSU) 1 degree × 1 degree V006*. Greenbelt, MD, USA: Goddard Earth Sciences Data and Information Services Center (GES DISC). [Available at <https://doi.org/10.5067/AQUA/AIRS/DATA301>, Accessed 19 September 2016].
- Aumann, H. H., Chahine, M. T., Gautier, C., Goldberg, M. D., Kalnay, E., McMillin, L. M., ... Susskind, J. (2003). AIRS/AMSU/HSB on the aqua mission: Design, science objectives, data products, and processing systems. *IEEE Transactions on Geoscience and Remote Sensing*, 41(2), 253–264. <https://doi.org/10.1109/TGRS.2002.808356>
- Bader, M., Forbes, G., Grant, J., Lilley, R., & Waters, A. (1995). *Images of Weather Forecasting: A Practical Guide for Interpreting Satellite and Radar Imagery*. Cambridge, UK: Cambridge University Press.
- Baylor, P. M., Jaffe, D. A., Pierce, R. B., & Gustin, M. S. (2016). Interannual variability in baseline ozone and its relationship to surface ozone in the western U.S. *Environmental Science & Technology*, 50(6), 2994–3001. <https://doi.org/10.1021/acs.est.6b00219>
- Bethan, S., Vaughan, G., Gerbig, C., Volz-Thomas, A., Richer, H., & Tiddeman, D. A. (1998). Chemical air mass differences near fronts. *Journal of Geophysical Research*, 103(D11), 13,413–13,434. <https://doi.org/10.1029/98JD00535>
- Bosilovich, M., Akella, S., Coy, L., Cullather, R., Draper, C., Gelaro, R., ... Suarez, M. (2015). MERRA-2: Initial evaluation of the climate. *NASA/TM-2015-104606*, 43, 139.
- Bosilovich, M. G., Lucchesi, R., & Suarez, M. (2016). MERRA-2: File specification GMAO Office Note No. 9 (Version 1.1). [Available at: <http://gmao.gsfc.nasa.gov/pubs/docs/Bosilovich785.pdf>, Accessed 20 June 2016].
- Browning, K. (1997). The dry intrusion perspective of extra-tropical cyclone development. *Meteorological Applications*, 4(4), 317–324.
- Büker, M. L., Hitchman, M. H., Tripoli, G. J., Pierce, R. B., Browell, E. V., & Avery, M. A. (2005). Resolution dependence of cross-tropopause ozone transport over East Asia. *Journal of Geophysical Research*, 110, D03107. <https://doi.org/10.1029/2004JD004739>
- Carlson, T. N. (1991). *Mid-Latitude Weather Systems*. New York, NY, USA: Routledge, Chapman Hall, Inc.
- Chahine, M. T., Pagano, T. S., Aumann, H. H., Atlas, R., Barnet, C., Blaisdell, J., ... Zhou, L. (2006). AIRS: Improving weather forecasting and providing new data on greenhouse gases. *Bulletin of the American Meteorological Society*, 87(7), 911–926. <https://doi.org/10.1175/BAMS-87-7-911>
- Cooper, O., Forster, C., Parrish, D., Dunlea, E., Höbler, G., Fehsenfeld, F., ... Horowitz, L. (2004). On the life cycle of a stratospheric intrusion and its dispersion into polluted warm conveyor belts. *Journal of Geophysical Research*, 109, D23S09. <https://doi.org/10.1029/2003JD004006>
- Cooper, O., Moody, J., Parrish, D., Trainer, M., Ryerson, T., Holloway, J., ... Evans, M. (2001). Trace gas signatures of the airstreams within North Atlantic cyclones: Case studies from the North Atlantic Regional Experiment (NARE '97) aircraft intensive. *Journal of Geophysical Research*, 106(D6), 5437–5456. <https://doi.org/10.1029/2000JD900574>, 2nd AGU Chapman Conference on Water Vapor in the Climate System, Potomac, Potomac, Maryland, Oct 12–15, 1999.
- Danielsen, E. F. (1968). Stratospheric-tropospheric exchange based on radioactivity, ozone and potential vorticity. *Journal of Atmospheric Sciences*, 25(3), 502–518.
- Danielsen, E. F. (1980). Stratospheric source for unexpectedly large values of ozone measured over the Pacific Ocean during Gametag, August 1977. *Journal of Geophysical Research*, 85(C1), 401–412. <https://doi.org/10.1029/JC085iC01p00401>
- Danielsen, E. F., & Mohnen, V. A. (1977). Project dustorm report: Ozone transport, in situ measurements, and meteorological analyses of tropopause folding. *Journal of Geophysical Research*, 82(37), 5867–5877. <http://dx.doi.org/10.1029/JC082i037p05867>
- Darmenov, A., & da Silva, A. (2015). The quick fire emissions dataset (QFED): Documentation of versions 2.1, 2.2 and 2.4 (NASA Technical Report Series on Global Modeling and Data Assimilation NASA TM-2015-104606, Volume 38).
- Dragani, R. (2011). On the quality of the ERA-Interim ozone reanalyses: Comparisons with satellite data. *Quarterly Journal of the Royal Meteorological Society*, 137(658), 1312–1326. <https://doi.org/10.1002/qj.821>
- EPA AirData (2016). [https://aqsdri.epa.gov/aqsweb/aqstmp/airdata/hourly_44201_2012.zip, Accessed 14 September 2016].
- Fischer, H., Wienhold, F. G., Hoor, P., Bujok, O., Schiller, C., Siegmund, P., ... Lelieveld, J. (2000). Tracer correlations in the northern high latitude lowermost stratosphere: Influence of cross-tropopause mass exchange. *Geophysical Research Letters*, 27(1), 97–100. <https://doi.org/10.1029/1999GL010879>
- Gelaro, R., McCarty, W., Suarez, M. J., Todling, R., Molod, A., Takacs, L., ... Zhao, B. (2017). The Modern-Era Retrospective Analysis for Research and Applications, Version 2 (MERRA-2). *Journal of Climate*, 30(14), 5419–5454. <https://doi.org/10.1175/JCLI-D-16-0758.1>
- Global Modeling and Assimilation Office (GMAO) (2015a). *MERRA-2 Inst3_3d_asm_Np: 3d,3-Hourly, Instantaneous, Pressure-Level, Assimilation, Assimilated Meteorological Fields V5.12.4*. Greenbelt, MD, USA: Goddard Space Flight Center Distributed Active Archive Center (GSFC DAAC). [<https://doi.org/10.5067/QBZ6MG944HW0>, Accessed 4/9/2016].
- Global Modeling and Assimilation Office (GMAO) (2015b). *MERRA-2 Tavg1_2d_slv_Nx: 2d,1-Hourly, Time-Averaged, Single-Level, Assimilation, Single-Level Diagnostics V5.12.4*. Greenbelt, MD, USA: Goddard Space Flight Center Distributed Active Archive Center (GSFC DAAC). [<https://doi.org/10.5067/VJAFPL1CSIV>, Accessed 11/8/2016].
- Global Modeling and Assimilation Office (GMAO) (2015c). *MERRA-2 Tavg1_2d_chm_Nx: 2d,1-Hourly, Time-Averaged, Single-Level, Assimilation, carbon Monoxide and Ozone Diagnostics V5.12.4*. Greenbelt, MD, USA: Goddard Space Flight Center Distributed Active Archive Center (GSFC DAAC). [<https://doi.org/10.5067/3RQ5YS674DG>, Accessed 11/8/2016].
- Global Modeling and Assimilation Office (GMAO) (2015d). *MERRA-2 Inst3_3d_asm_Nv: 3d,3-Hourly, Instantaneous, Model-Level, Assimilation, Assimilated Meteorological Fields V5.12.4*. Greenbelt, MD, USA: Goddard Space Flight Center Distributed Active Archive Center (GSFC DAAC). [<https://doi.org/10.5067/WWQSQ8VFVW8>, Accessed 4/10/2017].
- Herman, J. R., Hudson, R., McPeters, R., Stolarski, R., Ahmad, Z., Gu, X.-Y., ... Wellemeyer, C. (1991). A new self-calibration method applied to TOMS and SBUV backscattered ultraviolet data to determine long-term global ozone change. *Journal of Geophysical Research: Atmospheres*, 96(D4), 7531–7545. <https://doi.org/10.1029/90JD02662>
- Holton, J. R., Haynes, P. H., McIntyre, M. E., Douglass, A. R., Rood, R. B., & Pfister, L. (1995). Stratosphere-troposphere exchange. *Reviews of Geophysics*, 33(4), 403–439. <https://doi.org/10.1029/95RG02097>
- Hoskins, B., & Hodges, K. (2002). New perspectives on the Northern Hemisphere winter storm tracks. *Journal of Atmospheric Sciences*, 59(6), 1041–1061. [https://doi.org/10.1175/1520-0469\(2002\)059<1041:NPTNH>2.0.CO;2](https://doi.org/10.1175/1520-0469(2002)059<1041:NPTNH>2.0.CO;2)
- James, P., Stohl, A., Forster, C., Eckhardt, S., Seibert, P., & Frank, A. (2003). A 15-year climatology of stratosphere–troposphere exchange with a Lagrangian particle dispersion model 2. Mean climate and seasonal variability. *Journal of Geophysical Research*, 108(D12), 8522. <https://doi.org/10.1029/2002JD002639>
- Kaldunski, B., Pierce, B., & Holloway, T. (2017). When stratospheric ozone hits ground-level regulation: Exceptional events in Wyoming. *Bulletin of the American Meteorological Society*, 98(5), 889–892. <https://doi.org/10.1175/BAMS-D-14-00133.1>
- Knowland, K. E., Doherty, R. M., & Hodges, K. I. (2015). The effects of springtime mid-latitude storms on trace gas composition determined from the MACC reanalysis. *Atmospheric Chemistry and Physics*, 15(6), 3605–3628. <https://doi.org/10.5194/acp-15-3605-2015>

- Knowland, K. E., Doherty, R. M., Hodges, K. I., & Ott, L. E. (2017). The influence of mid-latitude cyclones on European background surface ozone. *Atmospheric Chemistry and Physics Discussion*, 2017, 1–39. <https://doi.org/10.5194/acp-2017-318>
- Krzyzanowski, M., & Cohen, A. (2008). Update of WHO air quality guidelines. *Air Quality, Atmosphere and Health*, 1, 7–13. <https://doi.org/10.1007/s11869-008-0008-9>
- Langford, A. O., Aikin, K. C., Eubank, C. S., & Williams, E. J. (2009). Stratospheric contribution to high surface ozone in Colorado during springtime. *Geophysical Research Letters*, 36, L12801. <https://doi.org/10.1029/2009GL038367>
- Langford, A. O., Brioude, J., Cooper, O. R., Senff, C. J., Alvarez, R. J., Hardesty, R. M., ... Oltmans, S. J. (2012). Stratospheric influence on surface ozone in the Los Angeles area during late spring and early summer of 2010. *Journal of Geophysical Research*, 117, D00V06. <https://doi.org/10.1029/2011JD016766>
- Langford, A. O., Masters, C. D., Proffitt, M. H., Hsie, E.-Y., & Tuck, A. F. (1996). Ozone measurements in a tropopause fold associated with a cut-off low system. *Geophysical Research Letters*, 23(18), 2501–2504. <https://doi.org/10.1029/96GL02227>
- Langford, A. O., Senff, C. J., Alvarez, R. J., Brioude, J., Cooper, O., Holloway, J., ... Williams, E. (2015). An overview of the 2013 Las Vegas Ozone Study (LVOS): Impact of stratospheric intrusions and long-range transport on surface air quality. *Atmospheric Environment*, 109, 305–322. <https://doi.org/10.1016/j.atmosenv.2014.08.040>
- Lefohn, A. S., Wernli, H., Shadwick, D., Limbach, S., Oltmans, S. J., & Shapiro, M. (2011). The importance of stratospheric–tropospheric transport in affecting surface ozone concentrations in the western and northern tier of the United States. *Atmospheric Environment*, 45(28), 4845–4857. <https://doi.org/10.1016/j.atmosenv.2011.06.014>
- Levelt, P. F., van den Oord, G. H. J., Dobber, M. R., Malkki, A., Visser, H., de Vries, J., ... Saari, H. (2006). The Ozone Monitoring Instrument. *IEEE Transactions on Geoscience and Remote Sensing*, 44(5), 1093–1101. <https://doi.org/10.1109/TGRS.2006.872333>
- Lin, M., Fiore, A. M., Cooper, O. R., Horowitz, L. W., Langford, A. O., Levy, H., ... Senff, C. J. (2012). Springtime high surface ozone events over the western United States: Quantifying the role of stratospheric intrusions. *Journal of Geophysical Research*, 117, D00V22. <https://doi.org/10.1029/2012JD018151>
- Lin, M., Fiore, A. M., Horowitz, L. W., Langford, A. O., Oltmans, S. J., Tarasick, D., & Rieder, H. E. (2015). Climate variability modulates western US ozone air quality in spring via deep stratospheric intrusions. *Nature Communications*, 6, 7105. <https://doi.org/10.1038/ncomms8105>
- Lin, M., Horowitz, L. W., Oltmans, S. J., Fiore, A. M., & Fan, S. (2014). Tropospheric ozone trends at Mauna Loa Observatory tied to decadal climate variability. *Nature Geoscience*, 7(2), 136–143.
- Lovill, J. E. (1970). The structure of gravity waves as determined simultaneously by ozone, temperature, and satellite data. *Archives for Meteorology, Geophysics, and Bioclimatology*, 19, 13–28.
- U.S. Environmental Protection Agency (2015). National ambient air quality standards for ozone: Final rule. *Federal Register*, 80(206), 65,292–65,468.
- McCarty, W., Coy, L., Gelaro, R., Huang, A., Merkova, D., Smith, E., ... Wargan, K. (2016). MERRA-2 input observations: Summary and assessment. *NASA/TM-2016-104606*, 46, 64p.
- McClain, E. P. (1960). Some effects of the western Cordillera of North America of cyclonic activity. *Journal of Meteorological*, 17(2), 104–115. [https://doi.org/10.1175/1520-0469\(1960\)017<0104:SEOTWC>2.0.CO;2](https://doi.org/10.1175/1520-0469(1960)017<0104:SEOTWC>2.0.CO;2)
- Monks, P. S. (2000). A review of the observations and origins of the spring ozone maximum. *Atmospheric Environment*, 34(21), 3545–3561.
- Nath, D., Chen, W., Graf, H.-F., Lan, X., Gong, H., Nath, R., ... Wang, L. (2016). Subtropical potential vorticity intrusion drives increasing tropospheric ozone over the tropical central Pacific. *Scientific Reports*, 6, 21370. <https://doi.org/10.1038/srep21370>
- Nieto, R., Sprenger, M., Wernli, H., Trigo, R. M., & Gimeno, L. (2008). Identification and climatology of cut-off lows near the tropopause. *Annals of the New York Academy of Sciences*, 1146(1), 256–290. <https://doi.org/10.1196/annals.1446.016>
- Olsen, M. A., Gallus, W. A., Stanford, J. L., & Brown, J. M. (2000). Fine-scale comparison of TOMS total ozone data with model analysis of an intense Midwestern cyclone. *Journal of Geophysical Research*, 105(D16), 20,487–20,495. <https://doi.org/10.1029/2000JD900205>
- Ott, L., Duncan, B., Pawson, S., Colarco, P., Chin, M., Randles, C., ... Nielsen, E. (2010). Influence of the 2006 Indonesian biomass burning aerosols on tropical dynamics studied with the GEOS-5 AGCM. *Journal of Geophysical Research*, 115, D14121. <https://doi.org/10.1029/2009JD013181>
- Ott, L. E., Duncan, B. N., Thompson, A. M., Diskin, G., Fasnacht, Z., Langford, A. O., ... Yoshida, Y. (2016). Frequency and impact of summertime stratospheric intrusions over Maryland during DISCOVER-AQ (2011): New evidence from NASA's GEOS-5 simulations. *Journal of Geophysical Research*, 121, 3687–3706. <https://doi.org/10.1002/2015JD024052>
- Palmén, E., & Newton, C. W. (1969). *Atmospheric Circulation Systems: Their Structure and Physical Interpretation* (603 pp.). New York: Academic Press.
- Reutter, P., Škerlak, B., Sprenger, M., & Wernli, H. (2015). Stratosphere–troposphere exchange (STE) in the vicinity of North Atlantic cyclones. *Atmospheric Chemistry and Physics*, 15(19), 10,939–10,953. <https://doi.org/10.5194/acp-15-10939-2015>
- Ryoo, J.-M., Johnson, M. S., Iraci, L. T., Yates, E. L., & Gore, W. (2017). Investigating sources of ozone over California using AJA airborne measurements and models: Assessing the contribution from long-range transport. *Atmospheric Environment*, 155, 53–67. <https://doi.org/10.1016/j.atmosenv.2017.02.008>
- Scherrer, S. C., Croci-Maspoli, M., Schwierz, C., & Appenzeller, C. (2006). Two-dimensional indices of atmospheric blocking and their statistical relationship with winter climate patterns in the Euro-Atlantic region. *International Journal of Climatology*, 26(2), 233–249. <https://doi.org/10.1002/joc.1250>
- Shapiro, M. A. (1974). A multiple structured frontal zone-jet stream system as revealed by meteorologically instrumented aircraft. *Monthly Weather Review*, 102(3), 244–253. [https://doi.org/10.1175/1520-0493\(1974\)102<0244:AMSFZJ>2.0.CO;2](https://doi.org/10.1175/1520-0493(1974)102<0244:AMSFZJ>2.0.CO;2)
- Shapiro, M. (1980). Turbulent mixing within tropopause folds as a mechanism for the exchange of chemical constituents between the stratosphere and troposphere. *Journal of Atmospheric Sciences*, 37(5), 994–1004.
- Škerlak, B., Sprenger, M., & Wernli, H. (2014). A global climatology of stratosphere–troposphere exchange using the ERA-Interim data set from 1979 to 2011. *Atmospheric Chemistry and Physics*, 14(2), 913–937. <https://doi.org/10.5194/acp-14-913-2014>
- Sprenger, M., & Wernli, H. (2003). A northern hemispheric climatology of cross-tropopause exchange for the ERA15 time period (1979–1993). *Journal of Geophysical Research*, 108(D12), 8521. <https://doi.org/10.1029/2002JD002636>
- Stohl, A., & Trickl, T. (1999). A textbook example of long-range transport: Simultaneous observation of ozone maxima of stratospheric and North American origin in the free troposphere over Europe. *Journal of Geophysical Research*, 104(D23), 30,445–30,462. <https://doi.org/10.1029/1999JD900803>
- Stohl, A., Wernli, H., James, P., Bourqui, M., Forster, C., Liniger, M. A., ... Sprenger, M. (2003). A new perspective of stratosphere-troposphere exchange. *Bulletin of the American Meteorological Society*, 84(11), 1565–1573.
- Susskind, J., Barnet, C., Blaisdell, J., Iredell, L., Keita, F., Kouvaris, L., ... Chahine, M. (2006). Accuracy of geophysical parameters derived from Atmospheric Infrared Sounder/Advanced Microwave Sounding Unit as a function of fractional cloud cover. *Journal of Geophysical Research*, 111, D09S17. <https://doi.org/10.1029/2005JD006272>

- US EPA AQS database (2017). [Available at <https://www.epa.gov/aqs>, Data extracted from the US EPA AQS database, Accessed 27 January 2017].
- Wargan, K., Labow, G., Frith, S., Pawson, S., Livesey, N., & Partyka, G. (2017). Evaluation of the ozone fields in NASA's MERRA-2 reanalysis. *Journal of Climate*, 30(8), 2961–2988. <https://doi.org/10.1175/JCLI-D-16-0699.1>
- Wargan, K., Pawson, S., Olsen, M. A., Witte, J. C., Douglass, A. R., Ziemke, J. R., ... Nielsen, J. E. (2015). The global structure of upper troposphere-lower stratosphere ozone in GEOS-5: A multiyear assimilation of EOS Aura data. *Journal of Geophysical Research: Atmospheres*, 120, 2013–2036. <https://doi.org/10.1002/2014JD022493>
- Waters, J. W., Froidevaux, L., Harwood, R. S., Jarnot, R. F., Pickett, H. M., Read, W. G., ... Walch, M. J. (2006). The Earth Observing System Microwave Limb Sounder (EOS MLS) on the Aura satellite. *IEEE Transactions on Geoscience and Remote Sensing*, 44(5), 1075–1092.
- Waugh, D. W., & Polvani, L. M. (2000). Climatology of intrusions into the tropical upper troposphere. *Geophysical Research Letters*, 27(23), 3857–3860. <https://doi.org/10.1029/2000GL012250>
- Wimmers, A. J., Moody, J. L., Browell, E. V., Hair, J. W., Grant, W. B., Butler, C. F., ... Ridley, B. A. (2003). Signatures of tropopause folding in satellite imagery. *Journal of Geophysical Research*, 108(D4), 8360. <https://doi.org/10.1029/2001JD001358>
- Yates, E. L., Iraci, L. T., Roby, M. C., Pierce, R. B., Johnson, M. S., Reddy, P. J., ... Gore, W. (2013). Airborne observations and modeling of springtime stratosphere-to-troposphere transport over California. *Atmospheric Chemistry and Physics*, 13(24), 12,481–12,494. <https://doi.org/10.5194/acp-13-12481-2013>
- Zanis, P., Hadjinicolaou, P., Pozzer, A., Tyrilis, E., Dafkà, S., Mihalopoulos, N., & Lelieveld, J. (2014). Summertime free-tropospheric ozone pool over the eastern Mediterranean/Middle East. *Atmospheric Chemistry and Physics*, 14(1), 115–132. <https://doi.org/10.5194/acp-14-115-2014>
- Zhang, L., Jacob, D. J., Yue, X., Downey, N. V., Wood, D. A., & Blewitt, D. (2014). Sources contributing to background surface ozone in the US Intermountain West. *Atmospheric Chemistry and Physics*, 14(11), 5295–5309. <https://doi.org/10.5194/acp-14-5295-2014>